Stem Cell Research & Therapy

RESEARCH

Open Access

Airway basal stem cell-derived extracellular vesicles modulate proliferation, migration and collagen deposition of fibroblasts

Lisi Luo[1,2,3†], Huijie Yang[1,3†], Junfeng Huang[1,3†], Difei Chen[1,3†], Yushan He[1,3], Jinsheng Lin[1,3], Haikang Zeng[1], Chu Hua[3,4], Zikai Lin[1,3], Minting Wu[1], Yuqin Ma[1,3], Qilin Deng[1,3], Ming Liu[1*] and Shiyue Li[1*]

Abstract

Background Human bronchial epithelial cell-derived extracellular vesicles have demonstrated the ability to attenuate fibroblasts activation. However, the specific key effector cell populations mediating this inhibitory effect remain unidentified. Airway basal stem cells (BSCs), which serve as progenitor cells for bronchial epithelial cells, play a critical role in fibrotic remodeling processes and possess significant therapeutic potential. This study aimed to characterize BSC-derived extracellular vesicles (BSC-EVs) and investigate their regulatory influence on fibroblasts behavior.

Methods Airway BSCs were collected through bronchoscopic brushing and differential centrifugation. Fibroblasts were subsequently treated with BSC-EVs at various concentrations to evaluate their dose- and time-dependent effects in vitro. The proteomic composition of BSC-EVs was analyzed using four-dimensional data-independent acquisition quantitative mass spectrometry (4D-DIA). Moreover, a bleomycin-induced pulmonary fibrosis model was established to evaluate the safety and preliminary efficacy of BSC-EVs.

Results We successfully isolated and identified BSC-EVs, which expressed the nucleus-specific marker TP63, indicative of BSCs, but lacked the BSC marker KRT5. Our findings demonstrated that BSC-EVs enhanced fibroblasts proliferation and migration in a dose-dependent manner. Importantly, BSC-EVs significantly attenuated fibroblasts activation and promoted fibroblasts senescence. Utilizing 4D-DIA quantitative proteomics, we revealed that BSC-EVs modulate extracellular matrix remodeling processes and regulate the expression of key proteins, including collagen I/III and matrix metalloproteinases. Animal models utilizing intratracheal administration of BSC-EVs demonstrate efficient reduction of collagen deposition.

†Lisi Luo, Huijie Yang, Junfeng Huang and Difei Chen contributed equally to this work

*Correspondence:
Ming Liu
mingliu@gzhmu.edu.cn
Shiyue Li
lishiyue@gzhmu.edu.cn

Full list of author information is available at the end of the article

Conclusion This study offers an extensive characterization of BSC-EVs, adhering to the guidelines set forth by MISEV2023. The findings underscore the significant therapeutic potential of BSC-EVs in the management of fibrotic diseases.

Keywords Airway basal stem cells, Extracellular vesicles, Fibroblasts

Background

Tissue fibrosis, characterized by fibroblasts activation and pathological extracellular matrix remodeling, is prevalent in respiratory diseases. For example, idiopathic pulmonary fibrosis (IPF) represents a progressive and irreversible condition with an unknown etiology [1], resulting in significant lung fibrosis and a high mortality rate. Current treatments, such as nintedanib and pirfenidone, exhibit limited efficacy [2]. Similarly, recurrent benign tracheal stenosis (BTS) is marked by repeated tracheal narrowing, leading to a diminished quality of life [3]. Although surgical resection is the primary therapeutic intervention, postoperative restenosis remains a major issue. It has been well established that fibroblasts behavior plays a crucial role in the fibrotic process, with their behavior shifting during different phases of healing [4]. In homeostasis, airway epithelial cells contribute to maintaining the mesenchymal–epithelial balance [5]. Due to the presence of the epithelial basement membrane, airway epithelial stem cells interact with fibroblasts indirectly through paracrine effect [6–8]. In response to injury, fibroblasts initially proliferate and migrate during the early phase, followed by a decline in proliferation and an increase in senescence during the remodeling stage to prevent excessive extracellular matrix deposition [9–11].

Recently, stem cell-based and derived therapies have garnered significant attention as promising therapeutic strategies for fibrosis-related respiratory conditions [12, 13]. Our recent study demonstrates that BSCs transplantation can inhibit granulation hyperplasia in BTS [14]. Moreover, the transplantation of SOX9 + airway basal stem cells (BSCs) into the airway has been shown to restore functional lung structure in adults [15]. Despite BSCs advantages in regulating tissue fibrosis and regeneration, cell-based therapy faces significant limitations, including immunogenicity, tumorigenicity, and ethical concerns [16]. Stem cells primarily exert their beneficial effects by releasing paracrine factors, such as extracellular vesicles (EVs) [17]. Compared to EVs derived from mesenchymal stem cells (MSCs), BSC-derived extracellular vesicles (BSC-EVs) may offer better targeting to epithelial and lung tissues for treating respiratory diseases [18, 19]. Although the anti-fibrotic properties of EVs derived from human bronchial epithelial cells or lung spheroid cells have demonstrated potential of for IPF treatment [20, 21], the mixed cell population, complicates the identification of the key contributing cells behind the therapeutic effect [22]. As the progenitor cell population of human bronchial epithelial cells, BSCs may play a critical therapeutic role in fibrosis. Therefore, we speculate that BSC-EVs may exhibit substantial anti-fibrotic effects and hold promise for the treatment of respiratory diseases.

A previous study isolated EVs from the immortalized human airway basal cell line, demonstrating their potential to enhance the survival of endothelial cells [23]. However, the role of immortalized cell lines may not adequately reflect individual heterogeneity, and anti-fibrotic effect remains poorly understood. Notably, airway BSC-EVs have exhibited therapeutic potential in IPF inhibiting epithelial-mesenchymal transition in activated lung cells [24]. Nevertheless, fundamental knowledge about BSC-EVs and their interactions with fibroblasts in fibrosis is still lacking. Fibroblast response to EVs is dependent on their cellular origin and dose [25]. The basic understanding of BSC-EVs and how fibroblasts respond to BSC-EVs at virous doses is crucial for both basic research and the clinical translation. This study aims to isolate and characterize BSC-EVs and to comprehensively investigate their impact on fibroblasts function and the underlying mechanisms.

Methods

Clinical samples and cell culture

Human airway tissue samples were obtained via bronchoscopy brushing from patients diagnosed with pulmonary nodules and BTS. Detailed donor characteristics are provided in Additional file 1 (Table S1). Then, human primary BSCs and fibroblasts were derived from these epithelial cells via differential centrifugation. More specifically, the epithelial cells were digested with 0.25% trypsin at 37 ℃ for one minute, and terminated digestion with DMEM medium containing FBS to obtain human primary fibroblasts. The cells remained adherent were human primary BSCs. Then, human primary fibroblasts were cultured in complete DMEM medium; and human primary BSCs were cultured in BSCs complete medium according to the patent (Chinese patent CN114958727B). Air-Liquid Interface (ALI) cultures of BSCs were conducted following established method [26]. Briefly, BSCs were seeded onto a transwell insert (filter pore size: 0.4 μm) at a density of 2 × 10^5 cells per well in 200 μL of ALI media, and 800 μL of ALI medium was added to the basal chamber for 28 days. The study received ethical approval from the Institutional Review Board of the First Affiliated Hospital of Guangzhou Medical University (Ethics Review Number ES-2024-K075-01).

Isolation, characterization and uptake experiments of BSC-EVs

Around 3×10^7 BSCs were cultured in a 5-layer cell factory (NEST, Wuxi, China), with 550 mL exosome-depleted medium and in a humidified atmosphere containing 5% CO_2. After 48–96 h, approximately 500 mL of culture media was collected, filtered (0.2 μm), and ultracentrifuged to isolate EVs. The BSC-EVs were resuspended in 500 μl of PBS and divided into five aliquots for storage at − 80℃. Human primary fibroblasts were then incubated with PKH26-labeled (Sigma, Saint Louis, Missouri, USA) BSC-EVs at various concentrations of 200, 2000, 10,000, 20,000, or 200,000 particles per cell for 24 h.

Cell proliferation and migration assay

Cell proliferation activity was assessed by cell counting kit-8 (CCK-8) assays. For the wound healing assay, fibroblasts were cultured in 6-well plates until nearly confluent, then treated with BSC-EVs at 200, 2000, 10,000, 20,000, or 200,000 particles/cell. Scratch wounds were made using sterile pipette tips, and gaps were recorded at 0 and 24 h. For the transwell assay, BSC-EVs treated fibroblasts were suspended in 150 μL serum-free culture medium and seeded into the upper compartment of a transwell plate (Corning, New York, USA). After 24 h of incubation at 37 °C, cells in the upper chamber were fixed with 4% paraformaldehyde and stained with 0.1% crystal violet.

Three-dimensional collagen gels and SA-β-Gal staining

Fibroblasts treated with varying doses of BSC-EV in serum-free medium were mixed with 3 mg/mL neutralized rat tail type I collagen at a 2:1 ratio. After 2 h at 37 °C to solidify the collagen, the gel's edges were detached from the well walls. The collagen-gel interface was then covered with 1 mL culture medium for 8 h at 37 °C. Fibroblasts were cultured in 24-well plates with BSC-EVs added at 200, 2000, 10,000, 20,000, or 200,000 particles/cell. Senescence associated β-galactosidase (SA-β-Gal) staining was performed according to the manufacturer's instructions (HUAYUN, Guangzhou, China). The area of each collagen gel was measured using ImageJ, and the gel area (%) was calculated as x/n (x = area of each group with cells, n = area of well).

RNA extraction and quantitative real-time PCR (qRT-PCR)

Total RNA was extracted using the TransZol Up Plus RNA Kit (Transgen, Beijing, China) according to the manufacturer's instructions. To investigate the expression of mRNA, reverse transcription was performed using the Hifair® III 1st Strand cDNA Synthesis SuperMix for qPCR (Yeasen). The amplification of qRT-PCR was assessed using Hieff UNICON® qPCR SYBR® Green Master Mix (Yeasen) on a CFX Connection Real-Time System (Bio-Rad, CA, USA). The relative expression of mRNA was normalized to GAPDH and calculated using the $2 - \Delta\Delta Ct$ method. Primers are listed in in Additional file 1 (Table S2).

Western blot analysis

Protein concentrations were measured using the BCA assay kit (Solarbio, Beijing, China). For SDS-PAGE, 20 μg of each protein extract was loaded and separated. Proteins were then transferred onto PVDF membranes (Beyotime, Shanghai, China) at 300 mA for 1 h. Membranes were blocked with 5% skimmed milk for 60 min and incubated with primary antibodies overnight at 4 °C, including CD9 (1:1000, SAB, Maryland, USA, 40708), CD63 (1:1000, SAB, 44012), CD81 (1:1000, SAB, 29677), TSG101 (1:1000, SAB, 49270), HSP70 (1:1000, SAB, 48597), KRT5 (1:1000, Abcam, Cambridge, UK, ab17130), P63 (1:1000, Abcam, ab124762), γ-H2A.X (1:1000, Abcam, ab9718), COL-1 (1:1000, Abcam, ab21286), α-SMA (1:1000, Abcam, ab5694), FAP (1:1000, CST, 66562), P16 (1:1000, CST, ab92803), P21 (1:1000, CST, ab2947), β-Tubulin (1:1000, Yeasen, 30301) or GAPDH (1:1000, CST). A 60-minute incubation at room temperature with secondary antibodies followed by three TBST washes. Additionally, the protein bands were detected by enhanced chemiluminescence, and quantitative analysis was performed utilizing ImageJ software.

Histology and Immunofluorescence staining

Fibroblasts treated with different BSC-EVs concentrations were seeded into 96-well plates. After fixing with 4% paraformaldehyde for 30 min at room temperature and rinsing with PBS, cells were permeabilized with 0.1% triton X-100 for 10 min, rinsed again, and blocked with 5% bovine serum albumin for 60 min. Primary antibodies, including KRT5 (1:200, Abcam, ab17130), P63 (1:200, Abcam, ab124762), Ki67 (1:200, Abcam, ab15580), MUC5AC (1:200, Abcam, ab3649), AC-TUB (1:200, Sigma, T6793) were applied overnight at 4 °C. Images were captured and analyzed using an inverted fluorescence microscope (Leica DMi8, Wetzlar, Germany). The Celigo Image Cytometer (Nexcellom Bioscience) was used to analyze fluorescence intensity, and Celigo Software Version 2.1 were utilized to quantification. Additionally, paraffin sections were stained with hematoxylin and eosin following standard histological procedures.

Animal experiment procedure, hematoxylin and Eosin, and Masson trichrome staining

Male C57BL/6 mice (8 ~ 10 weeks old, 20 ~ 25 g) were purchased from the Animal Experimental Center of Guangzhou Medical University and housed in a specific pathogen-free facility. All procedures involving animals were conducted in accordance with the protocol

approved by the Laboratory Animal Ethics Committee of Affiliated First Hospital of Guangzhou Medical University (No. 20240726). The experimental protocols complied with ARRIVE guidelines 2.0. A total of 18 mice were randomly divided into three groups ($n = 6$ for each group), including the PBS treated group (PBS), the bleomycin treated group (BLM) and the BLM plus BSC-EVs treated group (BLM + BSC-EVs). Body weight was monitored weekly throughout the study. For bleomycin treated mice, an intrathecal injection of bleomycin at a dose of 2 mg/kg was administered. The animal experiment spanned 21 days, during which mice were treated with 2e8 particles of BSC-EVs via intratracheal instillation on day 7, according to previously reported [24]. Mice were euthanized with an overdose of isoflurane inhalation and then euthanized by cervical dislocation on day 21, and their lung tissues were collected and fixed in 4% paraformaldehyde. HE staining was performed according to a standard protocol. Briefly, tissue sections were stained with hematoxylin solution for 5 min, followed by 5 dips in 1% acid ethanol and rinsed in distilled water. The sections were then stained with eosin solution for 3 min, followed by dehydration with graded alcohol and clearing in xylene. Masson trichrome staining was performed following a standard protocol and Ashcroft scoring was performed as described previously [27].

Proteomic analysis

Library sequencing was conducted on the Illumina HiseqTM 2500/4000 by Gene Denovo Biotechnology Co., Ltd (Guangzhou, China). For four-dimensional data-independent acquisition quantitative mass spectrometry (4D-DIA) quantitative proteomic analysis of exosomes, samples are concentrated via ultrafiltration, and proteins are precipitated with organic solvents. The precipitated proteins are then re-suspended, reduced, alkylated, and digested with trypsin. The peptides are analyzed using ultra-high pressure liquid chromatography and a mass spectrometer like orbitrap, utilliziing data-dependent acquisition for ion selection and fragmentation. Specialized software processes raw data to identify and quantify proteins, adhering to strict confidence criteria. This method maps the exosomal proteome, uncovering biological functions and potential biomarkers. Results are presented as mean ± standard deviation. The proteomics data in this study were included as an in Additional file 2. A two-tailed paired Student's t-test determines significance between groups, with $P \leq 0.05$ indicating statistical significance ($^{*}P \leq 0.05$; $^{**}P \leq 0.01$; $^{***}P \leq 0.01$).

Results

The characterization of BSC-EVs

The extraction of BSC-EVs was conducted successfully following the protocol outlined in Fig. 1. Initially, we demonstrated that BSCs exhibited high proliferation and activation capabilities using ALI cultures (Fig. 2A). The presence of BSC-EVs was subsequently confirmed through transmission electron microscopy (TEM) and Western blot analysis. TEM revealed the presence of classic cup-shaped vesicles, each with a diameter of less than 100 nm, within the BSC-EVs (Fig. 2B). These BSC-EVs

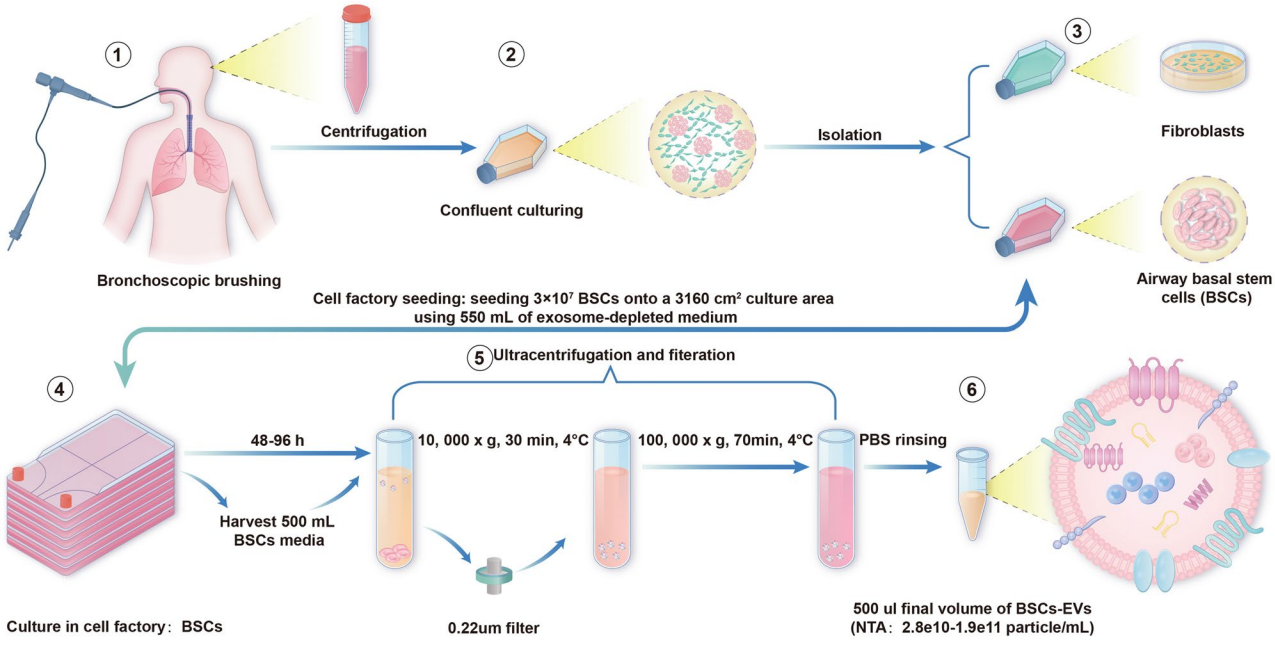

Fig. 1 The flowchart of BSC-EVs isolation

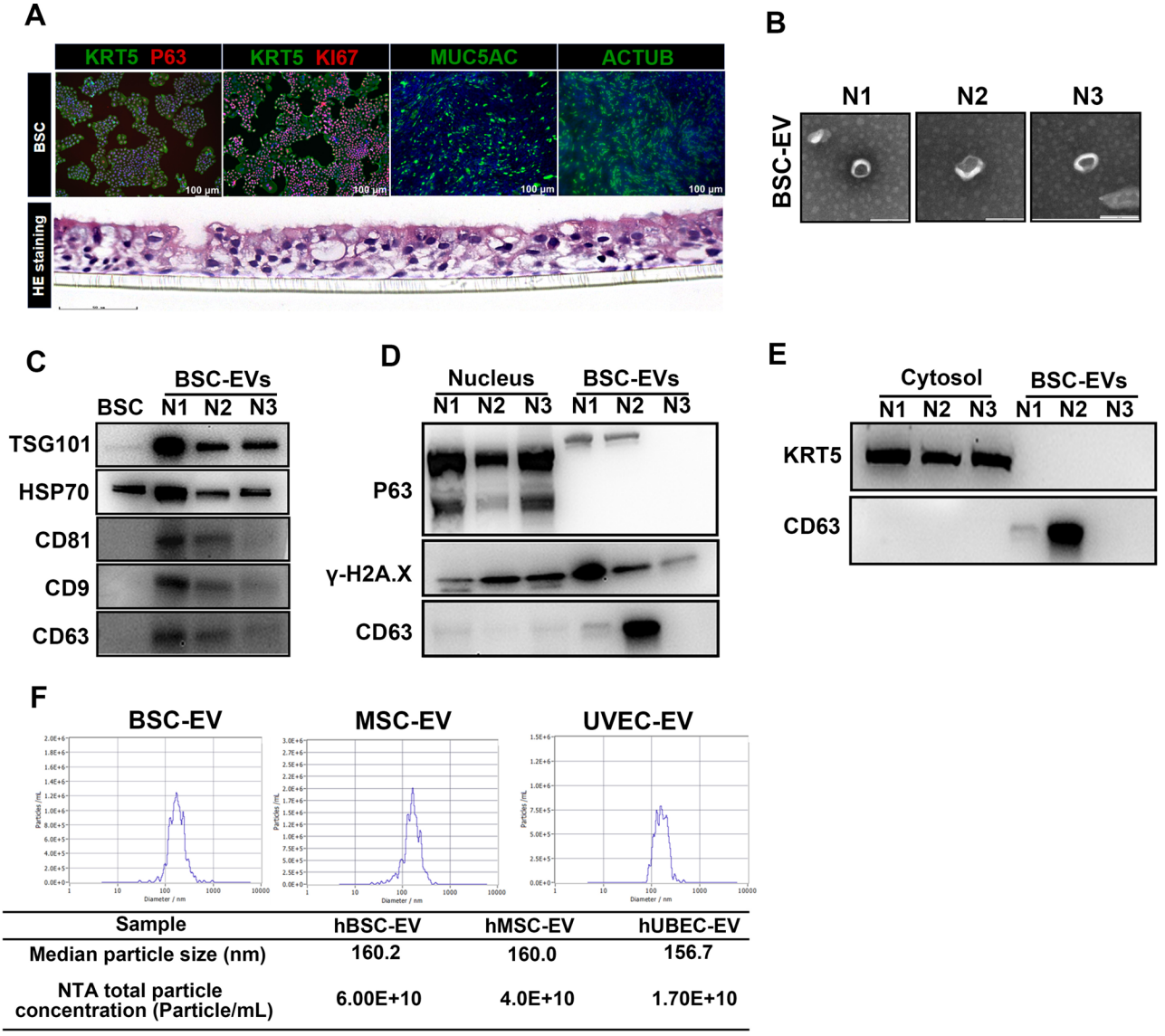

Sample	hBSC-EV	hMSC-EV	hUBEC-EV
Median particle size (nm)	160.2	160.0	156.7
NTA total particle concentration (Particle/mL)	6.00E+10	4.0E+10	1.70E+10

Fig. 2 Isolation and validation of BSC-EVs. (**A**) Representative images of BSC photographed by immunofluorescence and hematoxylin-eosin staining. (**B**) The cup-shaped particle evidence of BSC-EVs by TEM. (**C**) Exosomal markers (CD9, CD63, CD81, TSG101, HSP70) detection by western blot. Source blots are presented in Additional file 2: Fig. S1. (**D**-**E**) BSC markers (KRT5, TP63) and senescence marker of γ-H2A.X detection by western blot. Source blots are presented in Additional file 2: Fig. S2; (**F**) Comparison of sEVs derived from BSC, MSC and UVEC by Nanoparticle tracking analysis

expressed exosomal markers, including CD9, CD63, CD81, HSP70 and TSG101 (Fig. 2C and Additional file 2: Fig. S1), as well as the nuclear marker TP63, characteristic of BSCs, but did not express the BSC-specific marker KRT5 (Fig. 2D, E and Additional file 2: Fig. S2). Nanoparticle tracking analysis indicated that BSC-EVs exhibited a higher yield compared to EVs derived from mesenchymal stem cells and umbilical vein endothelial cells (6.0E + 10 vs. 4.0E + 10 vs. 1.7E + 10, respectively) (Fig. 2F).

BSC-EVs promote fibroblasts proliferation and migration, and senescence in a dose-dependent manner

To evaluate the responses of fibroblasts to varying doses of BSC-EVs, we conducted a comparative analysis of biological functions between control cells and those treated with BSC-EVs for a duration of 24 h (Fig. 3). Immunofluorescence analysis confirmed that fibroblasts internalized PKH26-labeled BSC-EVs, which were predominantly localized in the cytoplasm and perinuclear regions after 24 h (Fig. 4A). CCK-8 assays demonstrated that BSC-EVs significantly enhanced fibroblasts proliferation up to 72 h (Fig. 4B). Wound healing and transwell migration assays indicated that BSC-EVs promoted fibroblasts migration

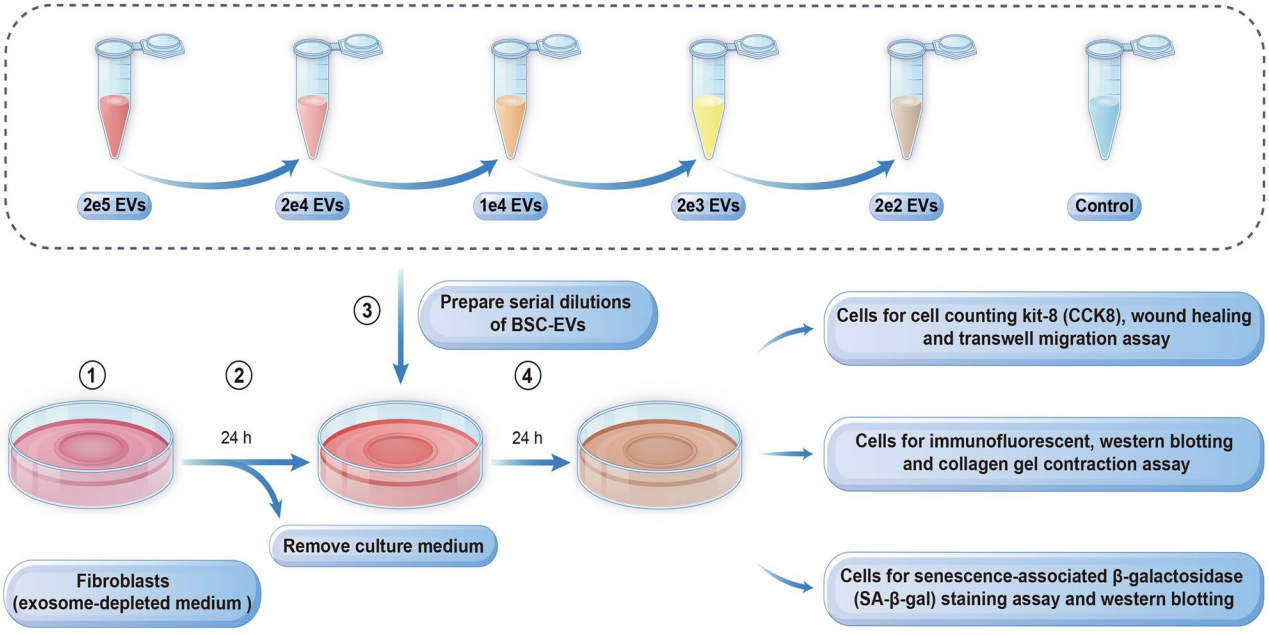

Fig. 3 Study design for proliferation, migration and collagen deposition of fibroblasts assays

after 24 h (Fig. 4C, D). Collectively, the CCK-8, wound healing, and transwell migration assays corroborated that BSC-EVs promote fibroblasts proliferation and migration in a dose-dependent manner.

The senescence marker γ-H2A.X was transferred from BSC-EVs to fibroblasts, inducing signs of senescence (Fig. 2E). Western blot analysis demonstrated increased expression of both P16 and P21, especially at a concentration of 2000 particles/cell (Fig. 4E and Additional file 2: Fig. S3). SA-β-Gal staining confirmed the induction of senescence, showing a higher proportion of senescent cells in the BSC-EV-treated group compared to the control (Fig. 4F). A key feature of senescent cells is the senescence-associated secretory phenotype (SASP). To further investigate this, qRT-PCR analysis revealed upregulation of several SASP factors, including chemokines (CCL2, CCL17), proinflammatory cytokines (IL-1α, IL-6), and metalloproteinases (MMP2, MMP9) in fibroblasts, consistent with the overall findings (Fig. 4G). Taken together, these results suggest that BSC-EVs induce a senescence response in fibroblasts.

BSC-EVs suppress fibroblasts proliferation and promote fibroblasts senescence in a time-dependent manner

To understand the context in which proliferation and senescence occur, we performed time-course experiments. First, we assessed fibroblasts proliferation at days 1, 3, 5, and 7. The CCK-8 assay revealed that fibroblasts proliferation was significantly slower in the BSC-EV-treated group compared to the control group after 3 days of incubation (Fig. 5A). Moreover, the protein levels of P16 and P21 were significantly elevated on day 7, indicating cell-cycle arrest and progression to cellular senescence (Fig. 5B and Additional File 2: Fig. 4). To further investigate whether BSC-EVs promote fibroblasts senescence over time, we performed β-galactosidase staining. The staining area in BSC-EV-treated fibroblasts was notably larger than in the control group, confirming that BSC-EVs induced senescence in a time-dependent manner (Fig. 5C). Additionally, qRT-PCR analysis revealed upregulation of multiple SASP factors, including CCL2, CCL17, IL-1α, IL-6, MMP2, and MMP9 in fibroblasts (Fig. 5D). Overall, our data indicate that BSC-EVs stimulate transiently accelerated fibroblasts proliferation during the initial 3 days, followed by a shift to proliferative arrest and cellular senescence starting on day 4.

BSC-EVs inhibit fibroblasts activation and induce senescence and attenuates bleomycin-induced lung fibrosis

Immunofluorescence analysis demonstrated that elevated quantities of BSC-EVs significantly reduced α-SMA expression, particularly at a concentration of 200,000 particles per cell ($p < 0.05$, Fig. 6A). No clear change of Ki67 fluorescence intensity was observed inside of the cells. Additionally, FAP levels decreased at 20,000 particles per cell, whereas collagen I expression was upregulated (Fig. 6B and Additional file 2: Fig. S5). BSC-EVs were found to inhibit fibroblasts activation in a dose-dependent manner, as evidenced by collagen contraction (all $p < 0.05$, Fig. 6C). Besides, western blot showed that the protein level of collagen I, and FAP were gradually reduced on 5, and 7 days after BSC-EVs treatment, paralleled with an induction of MMP2 (Fig. 6D and Additional

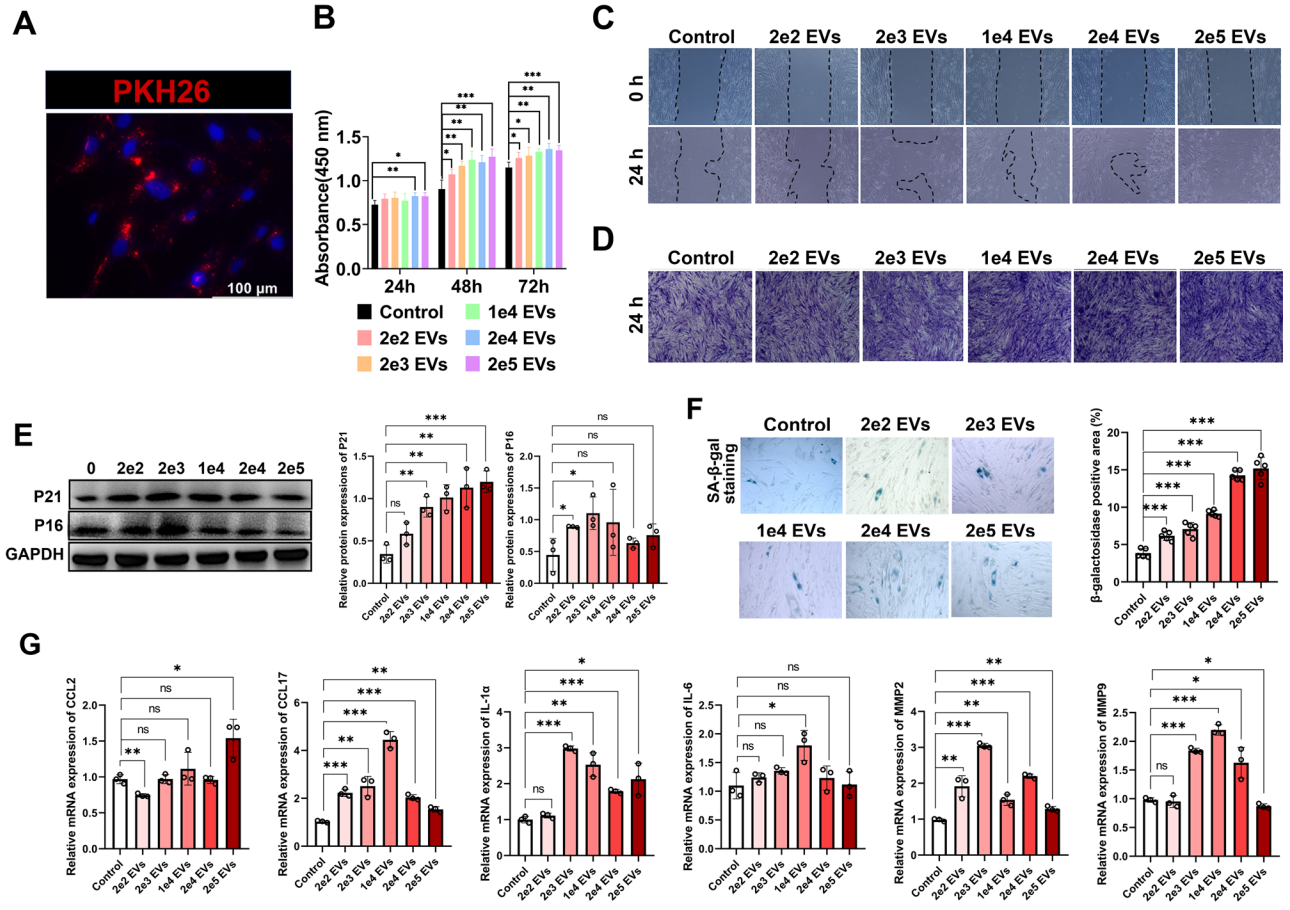

Fig. 4 BSC-EVs promote fibroblasts proliferation, migration, and senescence in a dose-dependent manner. (**A**) Representative fluorescent images of PKH26-labeled BSC-EVs for 24 h. Scale bars, 100 μm. (**B**) CCK-8 assay showing the effect of BSC-EVs on fibroblasts proliferation after a 24-, 48-, and 72-hours culture. (**C**-**D**) Wound healing and transwell migration assay of BSC-EVs treated fibroblasts at various concentrations of 200, 2000, 10,000, 20,000, or 200,000 particles per cell for 24 h. (**E**) Western blot analysis of p21 and p16 expression in BSC-EVs-treated fibroblasts for 48 h.
Source blots are provided in Additional File 2: Fig. S3. (**F**) Collagen gel contraction assay in BSC-EVs-treated fibroblasts. The area of each collagen gel was quantified using ImageJ software. (**G**) qRT-PCR analysis was performed to assess the relative mRNA expression levels of each SASP factor at 24 h, normalized to GAPDH mRNA levels. PBS-treated fibroblasts were used as a control.

file 2: Fig. S4). These findings collectively suggested that BSC-EVs inhibit fibroblasts activation in a time- and dose-dependent manner.

To further investigate the anti-fibrotic potential of BSC-EVs in the treatment of pulmonary fibrosis, we utilized a bleomycin-induced model of pulmonary fibrosis. Mice were successfully treated with 2e8 particles of BSC-EVs without any adverse effects, confirming the feasibility and safety of BSC-EV administration. Histological analysis, including Hematoxylin and Eosin and Masson's trichrome staining, revealed reduced collagen deposition and less damage to the alveolar septa in the BSC-EV-treated group compared to the bleomycin group (Fig. 6E). Additionally, Ashcroft scoring demonstrated significantly lower fibrosis severity in the BSC-EV-treated group compared to the bleomycin group, further corroborating the therapeutic effects of BSC-EVs (Fig. 6F). These results provide in vivo evidence supporting the potential of BSC-EVs as a promising therapeutic strategy for pulmonary fibrosis.

Proteome comparison between BSC-EVs and parent cells

A 4D-DIA quantitative proteomic analysis was performed to compare the protein composition of BSC-EVs and their parent cells (Additional file 3). Venn diagrams revealed that only a limited number of proteins in BSC-EVs were unique to their parental cells (Fig. 7A). Despite originating from individuals of varying sex, age, and disease conditions, the six BSCs exhibited remarkably similar proteomes (all Pearson's correlation > 0.8) (Fig. 7B). These findings suggest that BSCs may selectively load different cargoes into EVs. We subsequently conducted an analysis of the 1,000 most abundant proteins across six BSC-EV preparations, with a particular emphasis on 443 co-expressed proteins for Kyoto Encyclopedia of Genes

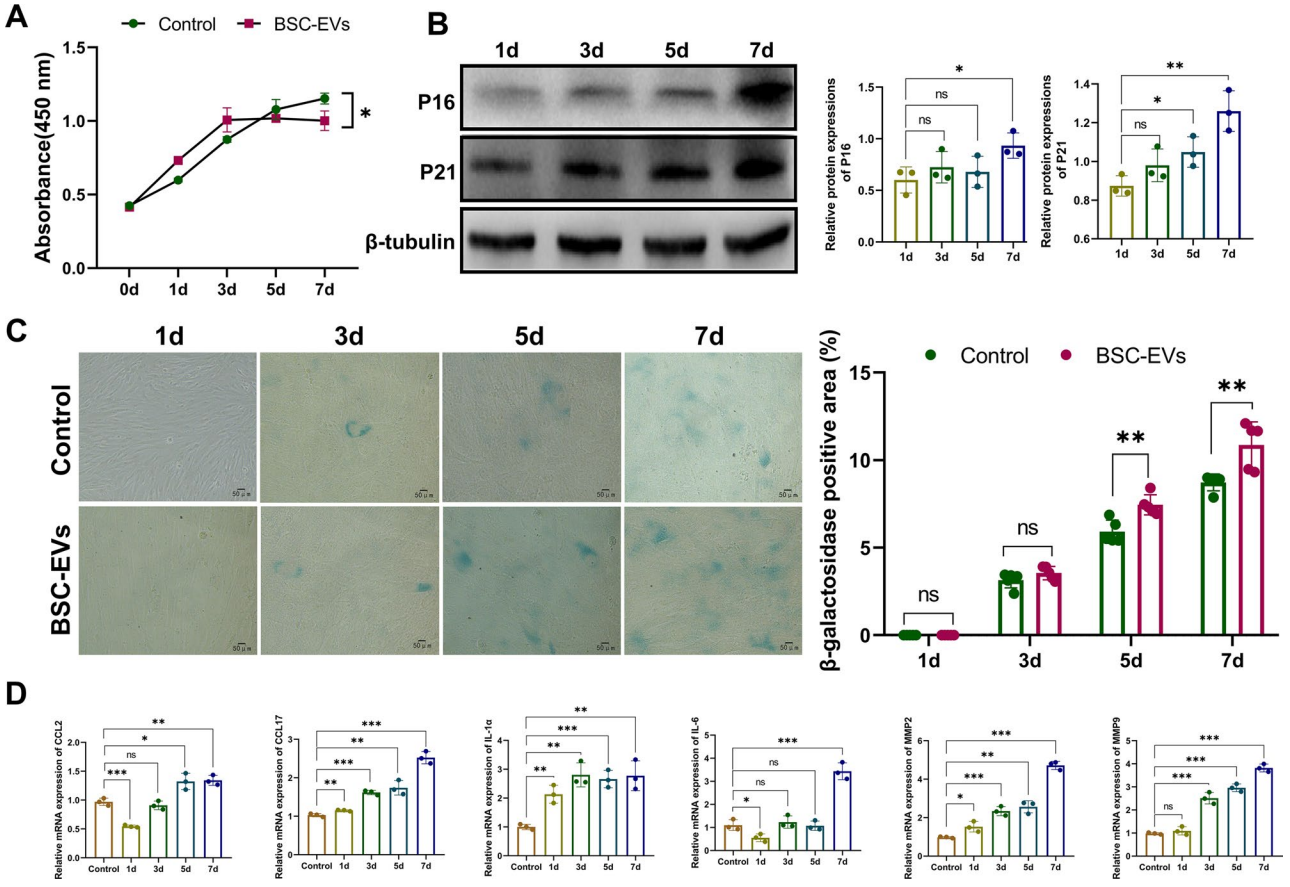

Fig. 5 BSC-EVs inhibit fibroblast proliferation and induce fibroblast senescence in a time-dependent manner. (**A**) Cell viability was assessed using the CCK-8 assay in the control PBS group and the BSC-EVs-treated group at 0, 1, 3, 5, and 7 days. (**B**) Western blot analysis of p16 and p21 expression in BSC-EVs-treated fibroblasts at 0, 1, 3, 5, and 7 days.
Source blots are provided in Additional file 2: Fig. S4. (**C**) SA-β-gal staining assays in the control PBS group and the BSC-EVs-treated group at 0, 1, 3, 5, and 7 days. The area of each collagen gel was quantified using ImageJ software. (**D**) qRT-PCR analysis was performed to assess the relative mRNA expression levels of each SASP factor, normalized to GAPDH mRNA levels. PBS-treated fibroblasts on day 1 were used as a control.

and Genomes (KEGG) pathway analysis and gene ontology (GO) enrichment analysis (Fig. 7C).

The KEGG pathway analysis revealed significant roles of EVs in processes such as endocytosis, tight junctions, focal adhesion, and ECM-receptor interaction (Fig. 8A). GO analysis indicated an enrichment in actin filament organization, cell junction assembly, and wound healing (Fig. 8B). The molecular functions identified were associated with cadherin/integrin/calcium-dependent protein binding, cytoskeletal structure, and cell adhesion (Fig. 8C). Key cellular components included focal adhesion, cell-substrate junctions, secretory granules/vesicles/endocytic lumen, and basal plasma membrane (Fig. 8D).

Protein composition of BSC-EVs related to ECM remodeling

Compared to BSCs, BSC-EVs exhibited significantly higher levels of CDH1 and CDH2, with a predominance of CDH1, suggesting epithelial-like signaling (Fig. 8E). To evaluate the impact of BSC-EVs on ECM remodeling, we analyzed the protein expression of collagen types I and III, as well as matrix metalloproteinases (MMPs) and a disintegrin and metalloproteinases (ADAMs). Our findings revealed that both the synthesis and degradation of ECM proteins were enhanced in the presence of BSC-EVs (Fig. 8F, H). These results indicate that BSC-EVs modulate ECM degradation in fibroblasts by transferring epithelial-like components, thereby influencing fibroblast-mediated ECM dynamics.

Discussion

BSC-EVs that conform to the MISEV2023 criteria, encapsulating the distinctive features of their source cells, particularly the TP63 marker. The findings further indicate a substantial regulatory role of BSC-EVs in modulating fibroblasts behavior, specifically by inhibiting fibroblasts activation and promoting senescence. We administered five doses to both EVs-untreated and EVs-treated fibroblasts. The observed inverse correlation between dosage and fibroblasts activation underscores the therapeutic potential of BSC-EVs. More importantly, our findings

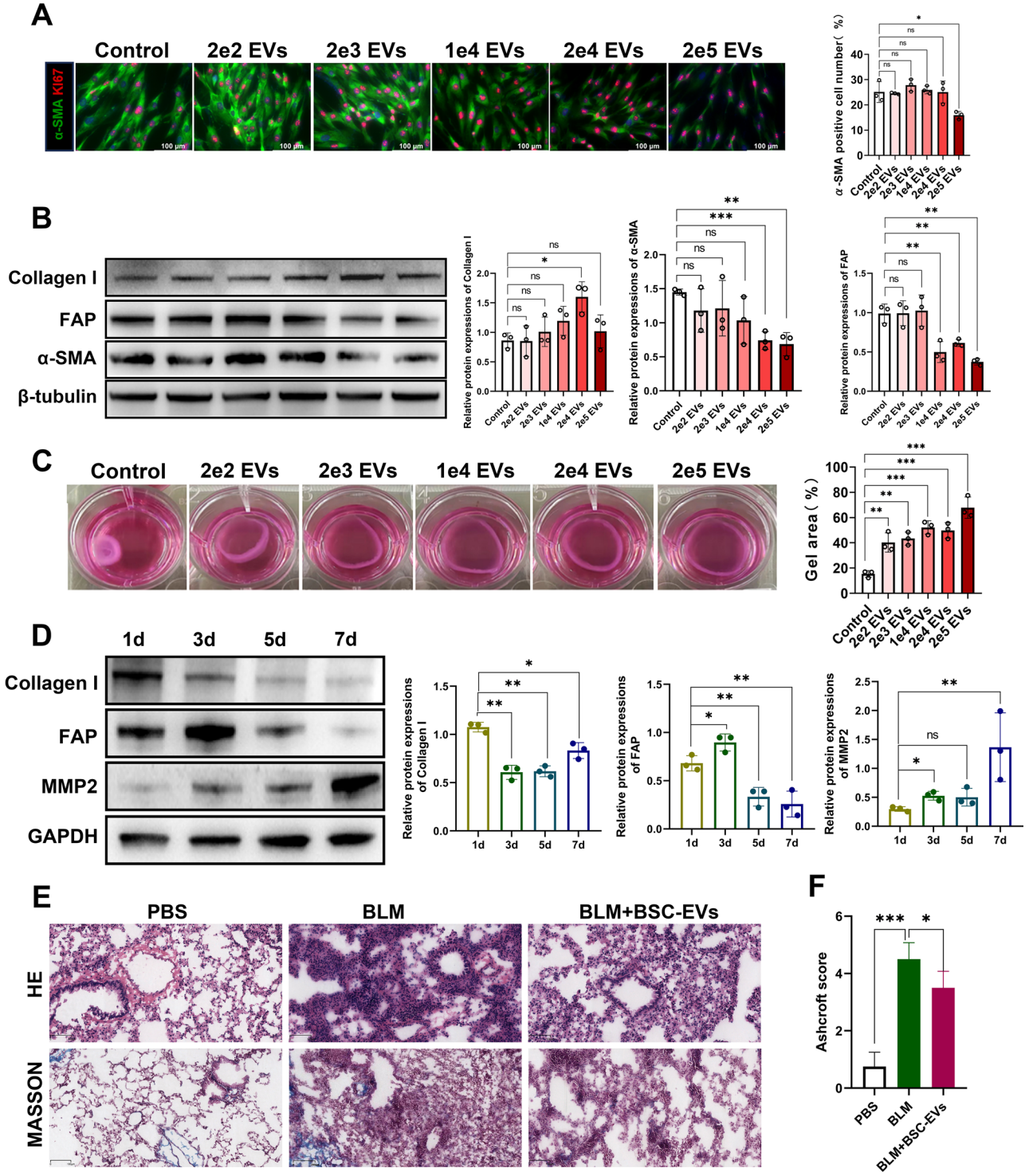

Fig. 6 BSC-EVs suppress fibroblasts activation in vitro and attenuates bleomycin-induced lung fibrosis in vivo. (**A**) Representative immunofluorescent images of α-SMA and KI67 expression in BSC-EVs treated fibroblasts. Quantification of α-SMA fluorescence intensity measured by Celigo Software. (**B**) Western blot for α-SMA, FAP, and collagen I in BSC-EVs treated fibroblasts. Source blots are presented in Additional file 2: Fig. S5; (**C**) Collagen gel contraction assay in BSC-EVs treated fibroblasts. The area of each collagen gel was quantified using ImageJ software. (**D**) Western blot for collagen I, FAP, and MMP2 in BSC-EVs treated fibroblasts at 0, 1, 3, 5, and 7 days. Source blots are presented in Additional file 2: Fig. S4. (**E**) Representative Hematoxylin and eosin and Masson trichrome staining. Scale bar = 100 μm. (**F**) Quantification of fibrosis by Ashcroft score; $n = 4$ biological independent animals. BLM: bleomycin

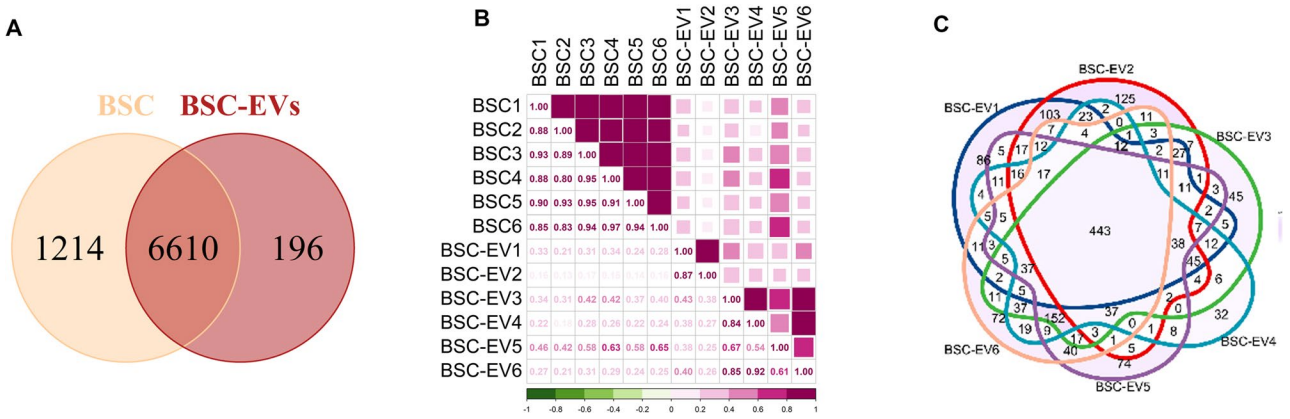

Fig. 7 Proteomic analysis of BSC-EVs by cell of origin. (**A**) Venn diagram of proteins identified in BSC-EVs derived from BSCs. (**B**) Correlation analysis of the protein contents of BSC-EVs and their source cells. (**C**) Venn diagram of BSC-EVs proteins derived from six donors

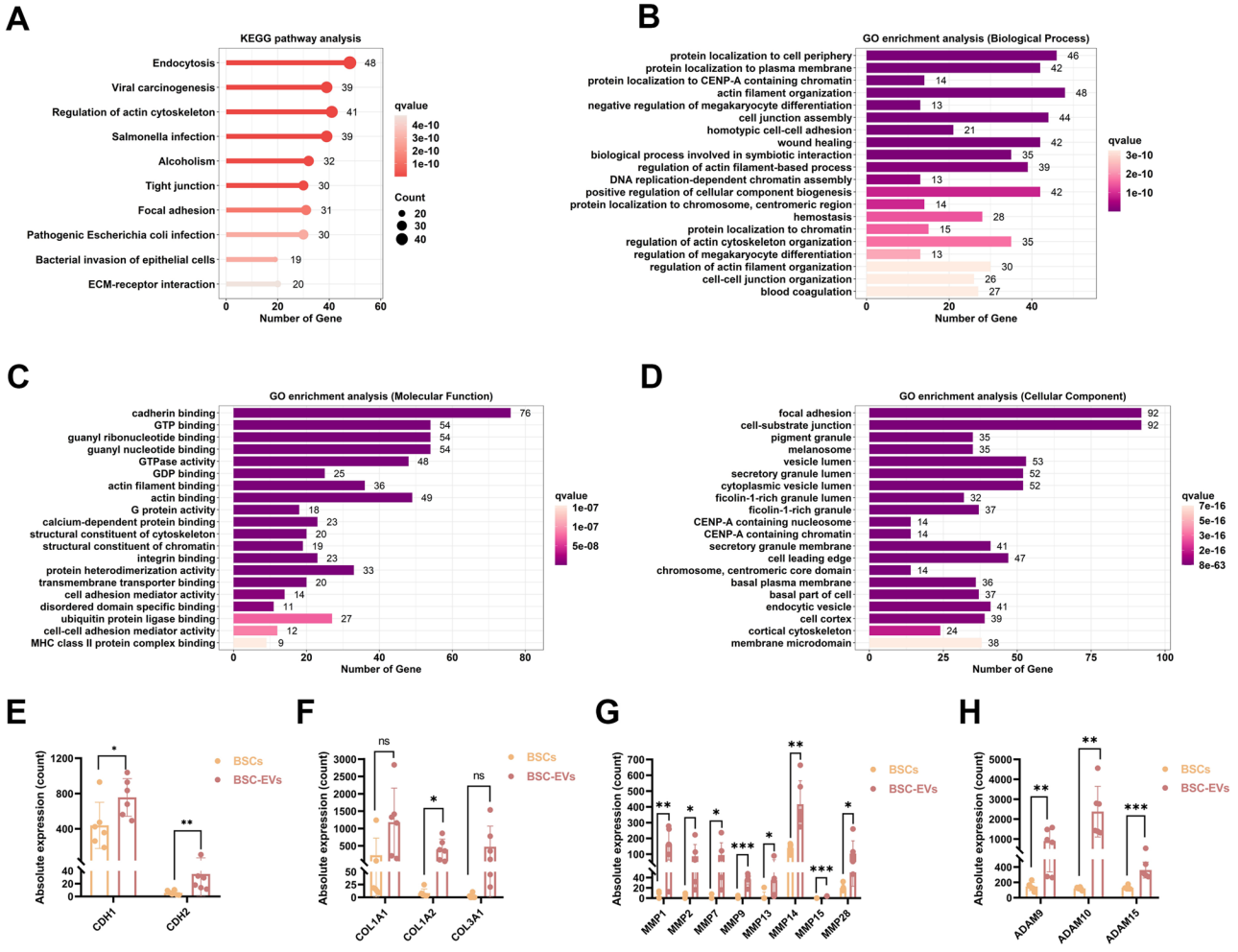

Fig. 8 Pathway enrichment and protein composition analysis of BSC-EVs. (**A**) KEGG pathway analysis of BSC-EVs. (**B**-**D**) GO analysis of biological process, molecular function, and cellular component terms associated with the BSC-EVs proteins. (**E**-**H**) Relative abundance of CDH1, CDH2, collagen I, collagen III, MMPs, and ADAMs proteins identified in all BSC-EVs

show that BSC-EVs facilitate collagen degradation in a time-dependent manner, suggesting the regulatory influence of BSC-EVs on fibroblast-mediated ECM remodeling. Proteomic analyses corroborated the upregulation of proteins associated with this process. Furthermore, we have established a bleomycin-induced pulmonary fibrosis model to provide preliminary evidence supporting the safety and therapeutic potential of BSC-EVs. Overall, this study underscores the potential therapeutic application of BSC-EVs in the treatment of respiratory fibrotic diseases.

In alignment with previous study [21], our study also showed that BSC-EVs could inhibit fibroblasts activation. Recent research posits that optimizing EV dosage is crucial for enhancing their therapeutic potential [25]. In our study, we utilized a range of 2e2 to 2e5 BSC-EV particles per cell to explore dose-response relationships, as referenced in prior studies [28, 29]. In comprehensive functional assays, fibroblasts function remained unchanged at 2e2 particles per cell, but effects emerged at 2e3 particles per cell and increased up to 2e4 particles per cell, with no further impact at concentrations up to 2e5 particles per cell. Administering excessively high doses may overload the endocytic machinery in a saturable manner, while excessively low doses could be ineffective [30]. Overall, BSC-EVs administered at doses between 2e2 and 2e5 particles per cell represent a reasonable therapeutic range for fibroblasts in vitro, with 2e4 particles per cell likely being the optimal dose in terms of cost-effectiveness. Notably, the doses of EVs used in in vitro experiments are relatively high compared to physiological levels [31]. In vivo studies on pulmonary fibrosis show significant effects with around 2e8 EV particles [32]. Additionally, a prior study reported patients with nebulized MSC-EVs at 2e8 to 1.6e9 particles reported no serious adverse events [33]. Thus, the 2e8 particle dose in this study seems appropriate. Given the dose-response effect, a dose-escalation approach could be beneficial in future clinical trials involving patients with idiopathic pulmonary fibrosis or benign tracheal stenosis. Overall, our findings suggest that BSC-EVs exert anti-fibrotic effects by suppressing fibroblasts activation, providing detailed insights into the dose-dependent responses of fibroblasts to BSC-EVs.

In the present study, we demonstrate that BSC-EVs effectively suppress fibroblasts activation at 2e4 particles per cell, whereas collagen I expression was also elevated at 48 h. The proteomic data provide a potential rationale for this observation, as collagen I proteins were detected within the cargo of BSC-EVs. It is well-documented that extracellular vesicles can carry different cargoes depending on clinical conditions [34]. A plausible explanation for the transient elevation in collagen levels is the uptake of BSC-EVs containing collagen I by recipient fibroblasts within the initial 48 h. In time-series experiments, western blot analysis demonstrated that collagen I protein levels exhibited a gradual decline over days 3, 5, and 7, suggesting collagen degradation. Overall, our data indicate that BSC-EVs initially facilitate the delivery of collagen I to recipient cells, resulting in a temporary elevation in collagen levels, which is subsequently followed by a transition towards collagen degradation at later stages.

On the other hand, our findings indicate that BSC-EVs can induce cellular senescence in fibroblasts. Several studies suggest that senescent lung fibroblasts may facilitate the differentiation of myofibroblasts, whereas other research indicates that fibroblasts senescence contributes to the wound healing response and tissue repair, thereby limiting fibrosis [35, 36]. Specifically, senescent fibroblasts play a crucial role in establishing a stem cell niche and are responsible for promoting the proliferation of BSCs and tissue repair in injury models [37, 38]. Overall, our finding pertaining that BSC-EVs induce fibroblasts senescence was consistent with these previous observations. In addition, our data indicate that BSC-EVs stimulate transiently accelerated fibroblasts proliferation during the initial phase, followed by a shift to proliferative arrest and cellular senescence starting on days 4. Notably, although the senescence marker γ-H2A.X was identified in the cargoes of BSC-EVs, no significant differences were observed between untreated ad treated groups. It is well-established that various stem cell-derived EVs influence cellular proliferation, thereby holding substantial promise for enhancing wound healing processes [39]. Correspondingly, treatment with BSC-EVs has demonstrated a marked improvement in both proliferation and migration, indicating potential benefits for tissue repair. Together, our findings suggest that BSC-EVs induce fibroblasts senescence, providing a novel perspective for fibrosis therapy.

EVs function as pivotal paracrine signaling entities, displaying a spectrum of bioactivities that are reflective of their cellular origins [40]. In this study, patients with benign lung nodules, normal lung function, and no history of smoking were selected. BSCs were obtained from the 3rd to 5th bronchial segments of healthy lungs, Proteomic analyses revealed that BSCs from different donors exhibited highly similar proteomes, suggesting minimal cellular heterogeneity following standardization strategies. In addition, our data revealed that BSC-EVs express the BSC-specific nuclear marker TP63, while lacking the other marker KRT5. Both TP63 and KRT5 are biomarkers of BSCs, but they serve distinct roles in cellular function. TP63 is not only a marker for progenitors but also plays a crucial role in lung regeneration, as well as in the expansion and survival of TP63 + progenitors during injury. Previous studies have highlighted that TP63 + BSCs are promising "seed cell" candidates for repairing damaged lung tissue, such as in chronic obstructive pulmonary

disease [41, 42]. In contrast, KRT5 is a cytoskeletal protein primarily responsible for maintaining epithelial cell integrity, with a more limited role in signal transduction [43]. Since EVs are secreted through signal transduction, they typically carry cargo involved in molecular regulation rather than structural components. Given the pivotal role of TP63 in epithelial regeneration, including in both airway and lung epithelia, we hypothesize that BSC-EVs may preferentially enrich TP63-related cargo over KRT5. This selective enrichment likely reflects the regenerative potential of BSC-EVs, linked to stemness properties and their ability to support tissue repair.

Despite these similarities at the cellular level, BSC-EVs demonstrated significant protein heterogeneity. It is documented that EV cargo composition can vary depending on clinical conditions [44]. Thus, a plausible explanation for the observed variability in BSC-EV cargo is the selective loading of specific molecules into EVs. To address the heterogeneity of BSC-EVs, future research could focus on two main aspects: (1) identifying the most functionally effective EV subtypes and (2) standardizing the production of engineered EVs [45, 46]. Improved functional characterization of specific BSC-EV subtypes will also contribute to the development of engineered BSC-EVs for therapeutic applications. KEGG and GO pathway analyses of BSC-EVs revealed significant enhancements in ECM-receptor interactions and wound healing processes. Extensive evidence indicates that MMPs play a therapeutic role in the degradation of ECM during fibrosis recovery [47, 48]. Consistent with these findings, our study observed the expression of MMP2 and MMP9 were elevated in fibroblasts following treatment with BSC-EVs, suggesting that BSC-EVs treatment facilitate collagen degradation. Additionally, enriched proteomic properties included cadherin/integrin/calcium-dependent protein binding and focal adhesion, indicative of epithelial signaling. A recent study proposed that modulating epithelial-mesenchymal transition might ameliorate fibrosis and enhance tissue repair [49]. The enrichment of CDH1 in BSC-EVs supports the potential anti-fibrotic effects of these vesicles, although further in vivo studies are necessary to fully validate these impacts. Together, our data demonstrate that BSC-EVs could upregulate the expression of MMP2/9 in fibroblasts, supporting their role in promoting excessive ECM degradation and facilitating fibrosis resolution.

Our study has several limitations. Firstly, the doses used in vivo were selected based on those reported in the literature, and the optimal mode of administration, dose, and frequency should be further refined. Additionally, future study should explore the potential long-term effects and safety concerns regarding BSC-EVs, including the versatility of the loaded cargo and non-targeted effects. Second, EVs are generally composed of proteins and microRNAs, but our data focus solely on proteins. Besides, the lack of knockdown or blocking experiments targeting specific proteins within BSC-EVs has limited us to explore further mechanistic details. In this study, the regulatory effect of BSC-EVs on fibroblasts appears to be partially mediated by protein cargo; however, further research is required to confirm the key miRNAs in BSC-EVs through miRNA sequencing and overexpression experiments targeting specific miRNAs within the BSC-EVs. Additionally, the potential mechanisms underlying fibroblast activation and collagen degradation need to be elucidated. Furthermore, nebulization therapy using engineered miRNA-enriched EVs may enable the precise delivery of bioactive components to the airways or lungs, making it a promising approach for treating respiratory diseases. In addition, this study exclusively demonstrated the regulatory effect of BSC-EVs on fibroblasts in vitro. The impact of EVs on ECM synthesis and degradation requires further validation in vivo. Third, the inherent heterogeneity of exosomes constrains our capacity to elucidate their mechanisms comprehensively. On the other hand, ultracentrifugation is limited in its ability to produce clinical-grade BSC-EVs for large-scale manufacturing processes. Given the limited number of BSCs obtained through bronchoscopy, we carefully consider both passage number and batch consistency. In future studies, high-throughput techniques such as tangential flow filtration, superabsorbent polymer beads, and size exclusion chromatography offer promising alternatives for improving the scalability and purification of BSC-EVs. Addressing these challenges, including heterogeneity, and scaling up BSC-EV production or application is critical to enhancing BSC-EV clinical applicability.

Conclusion

We successfully isolated and identified BSC-EVs, which expressed the nuclear marker TP63 but lacked the BSC marker KRT5. In comprehensive fibroblasts assays, BSC-EVs promoted fibroblasts proliferation, migration, and senescence while inhibiting fibroblasts activation in a dose- and time-dependent manner. Proteomic analysis of BSC-EVs indicated the activation of mechanisms associated with ECM remodeling, suggesting their potential anti-fibrotic properties. Animal experiments provide preclinical evidence supporting the clinical translation of BSC-EVs as a treatment strategy for fibrotic respiratory diseases, such as idiopathic pulmonary fibrosis. Overall, this study underscores the potential therapeutic application of BSC-EVs in the treatment of respiratory fibrotic diseases.

Abbreviations

IPF	Idiopathic pulmonary fibrosis
BTS	Benign tracheal stenosis
BSCs	Basal stem cells

EVs	Extracellular vesicles
BSC-EVs	BSC-derived extracellular vesicles
HBECs	Human bronchial epithelial cells
MSCs	Mesenchymal stem cells
UVEC	Umbilical vein endothelial cells
ECM	Extracellular matrix
MMPs	Matrix metalloproteinases (MMPs)
ADAMs	A disintegrin and metalloproteinases
ALI	Air-Liquid Interface
CCK-8	Cell Counting Kit-8
SA-β-Gal	Senescence associated β-galactosidase
SASP	Senescence-associated secretory phenotype
TEM	Transmission electron microscopy
4D-DIA	Four-dimensional data-independent acquisition quantitative mass spectrometry
KEGG	Kyoto Encyclopedia of Genes and Genomes pathway analysis
GO	Gene ontology analysis

Supplementary Information

The online version contains supplementary material available at https://doi.org/10.1186/s13287-025-04268-8.

Supplementary Material 1

Supplementary Material 2

Supplementary Material 3

Acknowledgements
The authors declare that artificial intelligence is not used in this study.

Author contributions
Study design: LL, HY, JH, DC; Methodology: YH, JL, HZ, CH; Data analysis and quality assessment: ZL, MW, YM, QD; Manuscript writing: LL, JH, DC; Project guidance and funding acquisition: ML, SL; All authors have read and approved the final manuscript.

Funding
This work was supported by Innovation team of respiratory diseases and regenerative medicine (2021KCXTD028), Zhongnanshan medical foundation of Guangdong Province (ZNSA-2020013), Clinical High-tech Project of Guangzhou (2023 C-GX04) and Guangdong Province Key Field Research and Development Program (2023B1111050006).

Data availability
The proteomics data supporting this study's findings are included as an Additional data file 3.

Declarations

Ethics approval and consent to participate
The study received ethical approval from the Institutional Review Board of the First Affiliated Hospital of Guangzhou Medical University (Ethics Review Number ES-2024-K075-01). The project title is "Exploration of the role and application of airway basal stem cell-derived extracellular vesicles (BSC-EVs) in respiratory diseases", and the approval date is 13/6/2024. Informed consent was obtained from all human subjects before their participation. All procedures involving animals were approved by the Laboratory Animal Ethics Committee of Affiliated First Hospital of Guangzhou Medical University (No. 20240726). Title of the approved project: Therapeutic effects and mechanisms of airway basal stem cell-derived extracellular vesicles (BSC-EVs) in pulmonary fibrosis repair, and the approval date is 4/9/2024.

Consent for publication
Not applicable.

Competing interests
The authors declare that they have no competing interests.

Author details
[1]Guangzhou Institute of Respiratory Health, State Key Laboratory of Respiratory Disease, National Clinical Research Center for Respiratory Disease, National Center for Respiratory Medicine, the First Affiliated Hospital of Guangzhou Medical University, Guangzhou, Guangdong, China
[2]Guangzhou National Laboratory, Guangzhou International Bio Island, No. 9 XingDaoHuanBei Road, Guangzhou 510005, Guangdong Province, China
[3]Guangzhou Medical University, Guangzhou, Guangdong, China
[4]Translatiaonl Research Centre of Regenrative Medicine and 3D Printing Technologies, Guangzhou Medical University, Guangzhou, China

Received: 4 October 2024 / Accepted: 6 March 2025
Published online: 18 March 2025

References

1. Raghu G, Collard HR, Egan JJ, Martinez FJ, Behr J, Brown KK, et al. An official ATS/ERS/JRS/ALAT statement: idiopathic pulmonary fibrosis: evidence-based guidelines for diagnosis and management. Am J Respir Crit Care Med. 2011;183(6):788–824. https://doi.org/10.1164/rccm.2009-040GL.
2. Wang J, Hu K, Cai X, Yang B, He Q, Wang J, et al. Targeting PI3K/AKT signaling for treatment of idiopathic pulmonary fibrosis. Acta Pharm Sinica B. 2022;12(1):18–32. https://doi.org/10.1016/j.apsb.2021.07.023.
3. Vergnon JM, Costes F, Polio JC. Efficacy and tolerance of a new silicone stent for the treatment of benign tracheal stenosis: preliminary results. Chest. 2000;118(2):422–6. https://doi.org/10.1378/chest.118.2.422.
4. Chen CY, Peng WH, Wu LC, Wu CC, Hsu SL. Luteolin ameliorates experimental lung fibrosis both in vivo and in vitro: implications for therapy of lung fibrosis. J Agric Food Chem. 2010;58(22):11653–61. https://doi.org/10.1021/jf1031668.
5. Zepp JA, Morrisey EE. Cellular crosstalk in the development and regeneration of the respiratory system. Nat Rev Mol Cell Biol. 2019;20(9):551–66. https://doi.org/10.1038/s41580-019-0141-3.
6. Conforti F, Ridley R, Brereton C, Alzetani A, Johnson B, Marshall BG, et al. Paracrine SPARC signaling dysregulates alveolar epithelial barrier integrity and function in lung fibrosis. Cell Death Discovery. 2020;6(54). https://doi.org/10.1038/s41420-020-0289-9.
7. Shiju TM, Sampaio LP, Hilgert GSL, Wilson SE. Corneal epithelial basement membrane assembly is mediated by epithelial cells in coordination with corneal fibroblasts during wound healing. Mol Vis. 2023;29:68–86.
8. Ruysseveldt E, Martens K, Steelant B. Airway basal cells, protectors of epithelial walls in health and respiratory diseases. Front Allergy. 2021;2(787128). https://doi.org/10.3389/falgy.2021.787128.
9. Lorena D, Uchio K, Costa AM, Desmoulière A. Normal scarring: importance of myofibroblasts. Repair Soc. 2002;10(2):86–92. https://doi.org/10.1046/j.1524-475x.2002.00201.x. Wound repair and regeneration: official publication of the Wound Healing Society [and] the European Tissue.
10. Guan R, Wang X, Zhao X, Song N, Zhu J, Wang J, et al. Emodin ameliorates bleomycin-induced pulmonary fibrosis in rats by suppressing epithelial-mesenchymal transition and fibroblast activation. Sci Rep. 2016;6(35696). https://doi.org/10.1038/srep35696.
11. Michalski J, Kanaji N, Liu X, Nogel S, Wang X, Basma H, et al. Attenuation of inhibitory prostaglandin E2 signaling in human lung fibroblasts is mediated by phosphodiesterase 4. Am J Respir Cell Mol Biol. 2012;47(6):729–37. https://doi.org/10.1165/rcmb.2012-0057OC.
12. Nakamura Y, Niho S, Shimizu Y. Cell-Based therapy for fibrosing interstitial lung diseases, current status, and potential applications of iPSC-Derived cells. Cells. 2024;13(11). https://doi.org/10.3390/cells13110893.
13. Cheng W, Zeng Y, Wang D. Stem cell-based therapy for pulmonary fibrosis. Stem Cell Res Ther. 2022;13(1):492. https://doi.org/10.1186/s13287-022-03181-8.
14. Ye YS, Chen DF, Liu M, Luo YL, Chen HJ, Zeng HK et al. Autologous airway basal cell transplantation alleviates airway epithelium defect in recurrent benign tracheal stenosis. Stem cells translational medicine 2023; 12 (12): 838–48. https://doi.org/10.1093/stcltm/szad062
15. Ma Q, Ma Y, Dai X, Ren T, Fu Y, Liu W, et al. Regeneration of functional alveoli by adult human SOX9(+) airway basal cell transplantation. Protein Cell. 2018;9(3):267–82. https://doi.org/10.1007/s13238-018-0506-y.
16. Zhang C, Zhang W, Zhu D, Li Z, Wang Z, Li J, et al. Nanoparticles functionalized with stem cell secretome and CXCR4-overexpressing

endothelial membrane for targeted osteoporosis therapy. J Nanobiotechnol. 2022;20(1):35. https://doi.org/10.1186/s12951-021-01231-6.
17. de Abreu RC, Fernandes H, da Costa Martins PA, Sahoo S, Emanueli C, Ferreira L. Native and bioengineered extracellular vesicles for cardiovascular therapeutics. Nat Reviews Cardiol. 2020;17(11):685–97. https://doi.org/10.1038/s41569-020-0389-5.
18. Mohan A, Agarwal S, Clauss M, Britt NS, Dhillon NK. Extracellular vesicles: novel communicators in lung diseases. Respir Res. 2020;21(1):175. https://doi.org/10.1186/s12931-020-01423-y.
19. Lee H, Zhang D, Zhu Z, Dela Cruz CS, Jin Y. Epithelial cell-derived microvesicles activate macrophages and promote inflammation via microvesicle-containing MicroRNAs. Sci Rep. 2016;6:35250. https://doi.org/10.1038/srep35250.
20. Li J, Sun S, Zhu D, Mei X, Lyu Y, Huang K, et al. Inhalable stem cell exosomes promote heart repair after myocardial infarction. Circulation. 2024;150(9):710–23. https://doi.org/10.1161/circulationaha.123.065005.
21. Kadota T, Fujita Y, Araya J, Watanabe N, Fujimoto S, Kawamoto H, et al. Human bronchial epithelial cell-derived extracellular vesicle therapy for pulmonary fibrosis via Inhibition of TGF-β-WNT crosstalk. J Extracell Vesicles. 2021;10(10):e12124. https://doi.org/10.1002/jev2.12124.
22. Duclos GE, Teixeira VH, Autissier P, Gesthalter YB, Reinders-Luinge MA, Terrano R, et al. Characterizing smoking-induced transcriptional heterogeneity in the human bronchial epithelium at single-cell resolution. Sci Adv. 2019;5(12):eaaw3413. https://doi.org/10.1126/sciadv.aaw3413.
23. Saxena A, Walters MS, Shieh JH, Shen LB, Gomi K, Downey RJ, et al. Extracellular vesicles from human airway basal cells respond to cigarette smoke extract and affect vascular endothelial cells. Sci Rep. 2021;11(1):6104. https://doi.org/10.1038/s41598-021-85534-6.
24. Gu X, Liu Z, Shan S, Ren T, Wang S. Airway basal cell–derived exosomes suppress epithelial–mesenchymal transition of lung cells by inhibiting the expression of ANO1. Experimental and therapeutic medicine 2024; 27 (5): 219. https://doi.org/10.3892/etm.2024.12507
25. Hagey DW, Ojansivu M, Bostancioglu BR, Saher O, Bost JP, Gustafsson MO, et al. The cellular response to extracellular vesicles is dependent on their cell source and dose. Sci Adv. 2023;9(35):eadh1168. https://doi.org/10.1126/sciadv.adh1168.
26. Lin LQ, Zeng HK, Luo YL, Chen DF, Ma XQ, Chen HJ, et al. Mechanical stretch promotes apoptosis and impedes ciliogenesis of primary human airway basal stem cells. Respir Res. 2023;24(1):237. https://doi.org/10.1186/s12931-023-02528-w.
27. Thomson EH. Ida W., Schuman, 1912–1977. J Hist Med Allied Sci. 1977;32(4):430–1. https://doi.org/10.1093/jhmas/xxxii.4.430.
28. Mathew B, Ravindran S, Liu X, Torres L, Chennakesavalu M, Huang CC, et al. Mesenchymal stem cell-derived extracellular vesicles and retinal ischemia-reperfusion. Biomaterials. 2019;197:146–60. https://doi.org/10.1016/j.biomaterials.2019.01.016.
29. Chutipongtanate S, Kongsomros S, Pongsakul N, Panachan J, Khowawisetsut L, Pattanapanyasat K, et al. Anti-SARS-CoV-2 effect of extracellular vesicles released from mesenchymal stem cells. J Extracell Vesicles. 2022;11(3):e12201. https://doi.org/10.1002/jev2.12201.
30. Gupta D, Zickler AM, El Andaloussi S. Dosing extracellular vesicles. Advanced drug delivery reviews 2021; 178 113961. https://doi.org/10.1016/j.addr.2021.113961
31. Otero-Ortega L, Laso-García F, Frutos MCG, Diekhorst L, Martínez-Arroyo A, Alonso-López E, et al. Low dose of extracellular vesicles identified that promote recovery after ischemic stroke. Stem Cell Res Ther. 2020;11(1):70. https://doi.org/10.1186/s13287-020-01601-1.
32. Dinh PC, Paudel D, Brochu H, Popowski KD, Gracieux MC, Cores J, et al. Inhalation of lung spheroid cell secretome and exosomes promotes lung repair in pulmonary fibrosis. Nat Commun. 2020;11(1):1064. https://doi.org/10.1038/s41467-020-14344-7.
33. Shi MM, Yang QY, Monsel A, Yan JY, Dai CX, Zhao JY, et al. Preclinical efficacy and clinical safety of clinical-grade nebulized allogenic adipose mesenchymal stromal cells-derived extracellular vesicles. J Extracell Vesicles. 2021;10(10):e12134. https://doi.org/10.1002/jev2.12134.
34. Schiavone S, Contursi A, Grande R, Patrignani P. Therapeutic targeting of dysregulated cellular communication. Annals Translational Med. 2017;5(10):222. https://doi.org/10.21037/atm.2017.03.62.
35. Jun JI, Lau LF. The matricellular protein CCN1 induces fibroblast senescence and restricts fibrosis in cutaneous wound healing. Nat Cell Biol. 2010;12(7):676–85. https://doi.org/10.1038/ncb2070.
36. Krizhanovsky V, Yon M, Dickins RA, Hearn S, Simon J, Miething C, et al. Senescence of activated stellate cells limits liver fibrosis. Cell. 2008;134(4):657–67. https://doi.org/10.1016/j.cell.2008.06.049.
37. Reyes NS, Krasilnikov M, Allen NC, Lee JY, Hyams B, Zhou M, et al. Sentinel p16(INK4a+) cells in the basement membrane form a reparative niche in the lung. Sci (New York NY). 2022;378(6616):192–201. https://doi.org/10.1126/science.abf3326.
38. Aros CJ, Vijayaraj P, Pantoja CJ, Bisht B, Meneses LK, Sandlin JM et al. Distinct Spatiotemporally dynamic Wnt-Secreting niches regulate proximal airway regeneration and aging. Cell stem cell 2020; 27 (3): 413–e429414. https://doi.org/10.1016/j.stem.2020.06.019
39. Wang Y, Zhang Y, Li T, Shen K, Wang KJ, Tian C, et al. Adipose mesenchymal stem cell derived exosomes promote keratinocytes and fibroblasts embedded in Collagen/Platelet-Rich plasma scaffold and accelerate wound healing. Adv Mater (Deerfield Beach Fla). 2023;35(40):e2303642. https://doi.org/10.1002/adma.202303642.
40. Kalluri R, LeBleu VS. The biology, function, and biomedical applications of exosomes. Sci (New York NY). 2020;367(6478). https://doi.org/10.1126/science.aau6977.
41. Lv Z, Liu Z, Liu K, Lin X, Pu W, Li Y, et al. Alveolar regeneration by airway secretory-cell-derived p63(+) progenitors. Cell Stem Cell. 2024;31(11):1685–e17001686. https://doi.org/10.1016/j.stem.2024.08.005.
42. Wang Y, Meng Z, Liu M, Zhou Y, Chen D, Zhao Y, et al. Autologous transplantation of P63(+) lung progenitor cells for chronic obstructive pulmonary disease therapy. Sci Transl Med. 2024;16(734):eadi3360. https://doi.org/10.1126/scitranslmed.adi3360.
43. LeFever NM, Katreddi RR, Dolphin NM, Mathias NA, Forni PE. Following the p63/Keratin5 basal cells in the sensory and non-sensory epithelia of the vomeronasal organ. Genesis (New York, NY: 2000) 2024; 62 (2): e23596. https://doi.org/10.1002/dvg.23596
44. Todorova D, Simoncini S, Lacroix R, Sabatier F, Dignat-George F. Extracellular vesicles in angiogenesis. Circul Res. 2017;120(10):1658–73. https://doi.org/10.1161/circresaha.117.309681.
45. Shen W, Guo K, Adkins GB, Jiang Q, Liu Y, Sedano S, et al. A single extracellular vesicle (EV) flow cytometry approach to reveal EV heterogeneity. Angewandte Chemie (International Ed English). 2018;57(48):15675–80. https://doi.org/10.1002/anie.201806901.
46. van de Wakker SI, Meijers FM, Sluijter JPG, Vader P. Extracellular vesicle heterogeneity and its impact for regenerative medicine applications. Pharmacol Rev. 2023;75(5):1043–61. https://doi.org/10.1124/pharmrev.123.000841.
47. Afratis NA, Klepfish M, Karamanos NK, Sagi I. The apparent competitive action of ECM proteases and cross-linking enzymes during fibrosis: applications to drug discovery. Adv Drug Deliv Rev. 2018;129:4–15. https://doi.org/10.1016/j.addr.2018.03.004.
48. de Haas HJ, Arbustini E, Fuster V, Kramer CM, Narula J. Molecular imaging of the cardiac extracellular matrix. Circul Res. 2014;114(5):903–15. https://doi.org/10.1161/circresaha.113.302680.
49. Youssef KK, Nieto MA. Epithelial-mesenchymal transition in tissue repair and degeneration. Nat Rev Mol Cell Biol. 2024;25(9):720–39. https://doi.org/10.1038/s41580-024-00733-z.

Publisher's note